Development of High Strength and Toughness Non-Heated Al–Mg–Si Alloys for High-Pressure Die-Casting

Ling-Yang Yuan[1] · Pan-Wen Han[1] · Ghulam Asghar[1] · Bao-Liang Liu[2] · Jin-Ping Li[3] · Bin Hu[3] · Peng-Huai Fu[1,2] · Li-Ming Peng[1,2]

Abstract

Based on the 3 factors and 3 levels orthogonal experiment method, compositional effects of Mg, Si, and Ti addition on the microstructures, tensile properties, and fracture behaviors of the high-pressure die-casting Al-xMg-ySi-zTi alloys have been investigated. The analysis of variance shows that both Mg and Si apparently influence the tensile properties of the alloys, while Ti does not. The tensile mechanical properties are comprehensively influenced by the amount of eutectic phase (α-Al + Mg_2Si), the average grain size, and the content of Mg dissolved into α-Al matrix. The optimized alloy is Al-7.49 Mg-3.08Si-0.01Ti (wt%), which exhibits tensile yield strength of 219 MPa, ultimate tensile strength of 401 MPa, and elongation of 10.5%. Furthermore, contour maps, showing the relationship among compositions, microstructure characteristics, and the tensile properties are constructed, which provide guidelines for developing high strength and toughness Al–Mg–Si–Ti alloys for high-pressure die-casting.

Keywords Al–Mg–Si–Ti alloy · Microstructure · Tensile properties · High strength and toughness · Contour maps

1 Introduction

In recent years, it has gradually become a new trend to use cast Al alloys in the automobile industry, especially for the cases of thin-walled parts with complex structures [1–4]. These structural components require not only high strength, but also high ductility (at least 10%) to meet the service conditions [5–8]. Therefore, it is extremely important to develop high-strength and high-ductility Al alloys that are suitable for high-pressure die-casting (HPDC). Dong et al. [9] found that HPDC Al-8.82Si-1.71Cu-0.4 Mg (wt%) alloy exhibits

the yield strength (YS) of 321 MPa, ultimate tensile strength (UTS) of 425 MPa, and elongation (EL.) of 11.3% after T6 heat treatment. Ji et al. [10, 11] also developed high quality HPDC Al alloys based on heat treatment. However, it is well known that heat treatment tends to cause dimensional instability of die castings. During heat treatment, gas in the die casting easily blisters, which leads to scraps of the castings. To overcome the drawbacks caused by heat treatment of Al alloys, it is indispensable to develop the non-heat-treated Al alloys with excellent comprehensive mechanical properties to broaden the practical applications of Al alloys for large complex thin-walled structural components.

HPDC Al–Mg–Si alloys are getting increasing attention in the automobile structure component due to their excellent mechanical properties [12–15]. To further develop HPDC Al–Mg–Si alloys with superior mechanical properties, microalloying is a suitable way. It has been reported that additions of Mg, Si, Fe, RE, Sc, and Ni elements in Al–Mg–Si alloys obviously improve the mechanical properties [16–22]. For example, Magsimal®-59 (Al–Mg–Si) alloy [14] exhibits excellent tensile properties by strictly controlling Fe content (< 0.15 wt%). The YS, UTS, and EL. of the alloy are about 160 MPa, 300 MPa, and 15%, respectively. Zhang et al. [16] also developed a high strength

✉ Li-Ming Peng
plm616@sjtu.edu.cn

1 National Engineering Research Center of Light Alloy Net Forming and Key State Laboratory of Metal Matrix Composites, School of Materials Science and Engineering, Shanghai Jiao Tong University, Shanghai 200240, China

2 Shanghai Light Alloy Net Forming National Engineering Research Center Co., Ltd, Shanghai 201615, China

3 General Motors China Science Laboratory, Shanghai 201206, China

and ductility Al-5 Mg-0.7Mn-0.3Si (wt%) alloy for high-pressure die-casting. Hu et al. [17] investigated the effect of Mg content (5.7–7.2 wt%) on the mechanical properties of Al–Mg–Si–Mn alloy. Ji et al. [18] reported that Al-(5.0–5.5) Mg-(1.5–2.0)Si alloys containing 0.5–0.7 Mn, 0.15–0.2 Ti, and 0.25 Fe (wt%) exhibit higher tensile strengths and ductility. The previous investigations focused on the optimization of alloying elements to improve the mechanical properties. In contrast, the effect of the alloying elements on the microstructures and the relationship between microstructures and tensile properties has not been studied in detail.

The microstructure of HPDC Al–Mg–Si alloys generally consists of the α-Al matrix with dissolved Mg atoms and (α-Al + Mg_2Si) eutectic phase [23–26]. Therefore, solid solution strengthening and dispersed secondary phase strengthening are the main contributions to the mechanical properties. As the degree of solid solution and fraction of eutectic phase change with the alloy compositions, which in turn affect the mechanical properties, it is important to explore the relationship among compositions, microstructures, and tensile properties of Al–Mg–Si alloys. Development of HPDC Al–Mg–Si alloys with EL. > 10%, YS > 200 MPa, and UTS > 400 MPa would stimulate further applications of Al alloys for car body structural components.

This work aims to study the effect of Mg, Si, and Ti alloying elements on HPDC Al–Mg–Si alloys based on the orthogonal experiment design to develop new high-pressure die-casting Al–Mg–Si alloys with comprehensive mechanical properties. The relationship among chemical compositions, microstructures, and tensile properties of Al–Mg–Si alloys for HPDC was also discussed in detail.

2 Selection Criteria of Mg and Si in the Experiment

Thermal dynamic calculation of equilibrium phase diagram of Al–Mg–Si alloys was conducted using Pandat software. The selection criterion was set to obtain HPDC Al–Mg–Si alloys with sufficient tensile properties and good casting performance. The weight ratio of Mg content to Si content was controlled as more than 1.73 to obtain the (α-Al + Mg_2Si) eutectic [27]. When Mg content was set as 5.5, 6.5, and 7.5 (wt%), the Si content was controlled in the range of 0.5–3, 0.5–3.76, and 0.5–4.3 (wt%), respectively. Moreover, 0.6 wt% Mn was added in the alloys during the calculation process as to approaching the actual alloy composition. Usually, Fe content is kept below 0.15 wt% to reduce the formation of needle-shaped iron-containing phases to achieve high-toughness of HPDC aluminum alloys. Mn (0.5–0.8 wt%) is used to replace the Fe and prevent the die-sticking.

Fig. 1 shows the vertical section of Al-5.5 Mg-Si-0.6Mn-0.15Ti equilibrium phases diagram with Si content in the
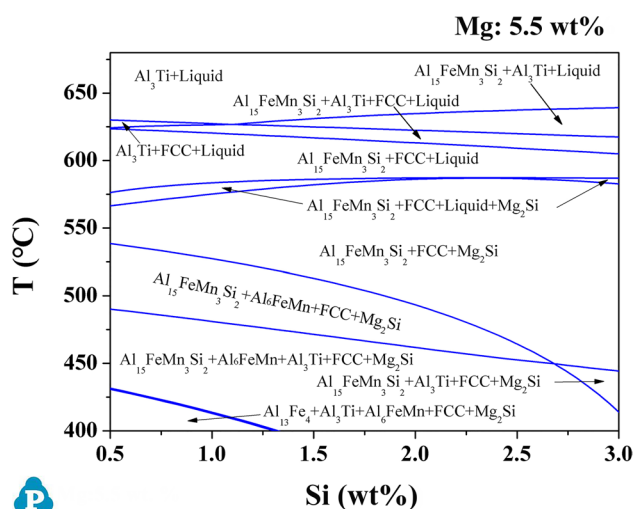
Fig. 1 Vertical section of Al-5.5 Mg-Si-0.6Mn-0.15Ti (wt%) equilibrium phases diagram with Si content in the range of 0.5–3.0 wt% calculated with Pandat software

range of 0.5–3.0 wt%, calculated with Pandat. For the associated alloy compositions, 4 compounds are involved, *i.e.*, Al_3Ti phase, Fe-containing phase, FCC (α-Al), and (α-Al + Mg_2Si) eutectic phase, during solidification process.

The typical solidification process of the Al–Mg–Si alloy is shown in Fig. 2a. In addition, the solidification range (ΔT), the content of Mg dissolved into matrix (M), and the proportion of eutectic (E) of the alloys are calculated by Pandat software, as shown in Fig. 2b-d. It can be found that ΔT, M, and E vary with the changes of Mg and Si content. In order to obtain 35–55% eutectic phase, more than 1 wt% Mg in matrix and narrow solidification range, Mg and Si additions are selected to be 6.5–7.5 and 2.0–3.0 (wt%), respectively.

3 Experimental

The orthogonal experimental design of the 3 factors and 3 levels ($L_9(3^3)$), which optimizes the number of castings, is listed in Table 1. According to Sect. 2, the contents of Mg and Si are within the range of 6.5–7.5 wt% and 2.0–3.0 wt%, respectively. Ti is further added for the purpose of grain refinement, where the addition of Ti is within the range of 0–0.2 wt%. The contents of Mg, Si, and Ti are selected as factor *A, B,* and *C*, respectively. As can be seen in Table 1, the 3 levels for factor *A* (Mg addition), factor *B* (Si addition), and factor *C* (Ti addition) are 6.5–7.0–7.5, 2.0–2.5–3.0, and 0–0.1–0.2, respectively. In addition, an error column in the orthogonal table is denoted as *D*.

In this work, the interaction of the three factors (Mg, Si, Ti) is not considered. It should be noted that the range of alloy compositions selected in the orthogonal experiment
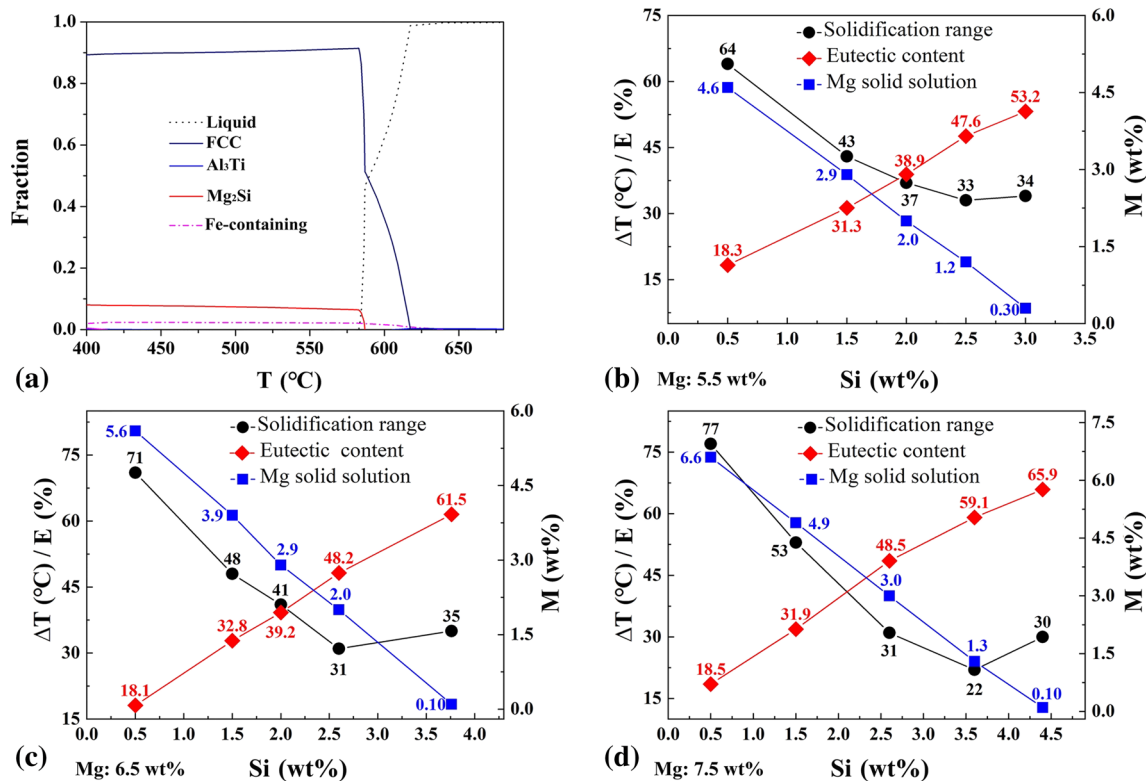
Fig. 2 **a** Solidification process of the Al–Mg–Si alloy; and **b–d** solidification range (ΔT), content of Mg dissolved into the matrix (M) and the proportion of eutectic compounds (E) for **b** Al-5.5 Mg (0.5–3.0)Si, **c** Al-6.5 Mg-(0.5–3.76)Si, and **d** Al-7.5 Mg-(0.5–4.3)Si alloys

Table 1 3 factors and 3 levels orthogonal design of HPDC Al-xMg-ySi-zTi alloys

| Symbol	A	B	C	D	Tensile properties
	Mg (wt%)	Si (wt%)	Ti (wt%)	e	
1#	1 (6.5)	1 (2.0)	1 (0.0)	1	
2#	1 (6.5)	2 (2.5)	2 (0.1)	2	
3#	1 (6.5)	3 (3.0)	3 (0.2)	3	
4#	2 (7.0)	1 (2.0)	2 (0.1)	3	
5#	2 (7.0)	2 (2.5)	3 (0.2)	1	
6#	2 (7.0)	3 (3.0)	1 (0.0)	2	
7#	3 (7.5)	1 (2.0)	3 (0.2)	2	
8#	3 (7.5)	2 (2.5)	1 (0.0)	3	
9#	3 (7.5)	3 (3.0)	2 (0.1)	1	

is very small (6.5–7.5 wt% Mg, 2–3 wt% Si, 0–0.2 wt% Ti). Therefore, it is uncertain whether Mg, Si, and Ti have interaction on the microstructures and tensile properties of the HPDC Al-xMg-ySi-zTi alloys within the change of alloy compositions. Considering the time and cost of alloys development, out of 27 alloy compositions ($L_{27}(3^{13})$), 9 alloy compositions ($L_9(3^3)$) are selected for die-casting experiments.

The analysis of variance (ANOVA) technique was used to process the results of orthogonal experiment. For the ANOVA, the test results can be decomposed into data fluctuations caused by factor/levels or experimental errors. F values will be applied to determine the significance of each factor on the results. In order to reveal the relationship among chemical compositions, microstructures, and tensile properties, Minitab software was employed to conduct multiple regression analysis. The significance of the regression coefficient, which shows the influence degree of the predictors on the response variable, was determined by the F-test.

The Al–Mg–Si–Ti alloys were melted in an electrical resistance furnace using pure Al, Mg, and Al-20Si (wt%), Al-10Mn (wt%), and Al-5Ti-B (wt%) master alloys. A TOYO-BD350V5 cold chamber HPDC machine was used to produce castings with dimensions as shown in Fig. 3 under the same filling parameters (shown in Fig. 4). The mold and pouring temperatures were set to be 200 ˚C and 700 ˚C, respectively. After casting, the tensile specimens (diameter × gauge length = 6.4 mm × 50 mm) were directly quenched into the warm water (about 60 ˚C). The chemical compositions of the castings were determined by using Optima 7300DV inductively coupled plasma (ICP) analysis, and the results are listed in Table 2.

Tensile tests were conducted using a universal testing machine (Zwick/Roell-Z100), with a knife-edge
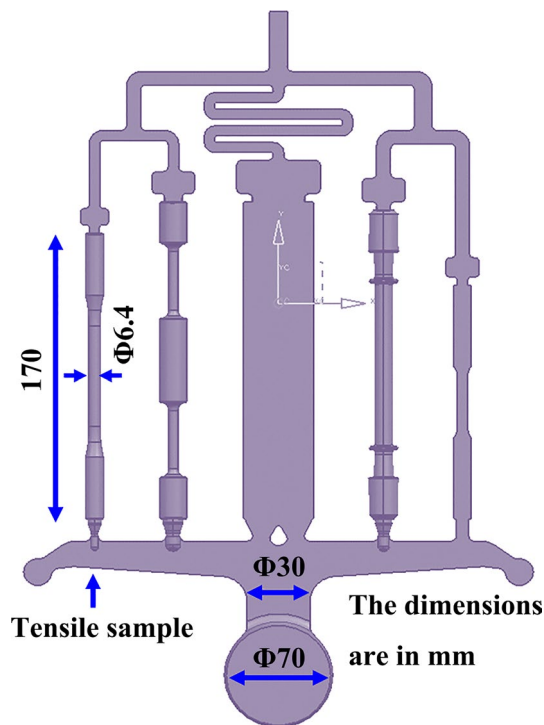
Fig. 3 Dimension and shape of the sample castings produced by high-pressure die-casting
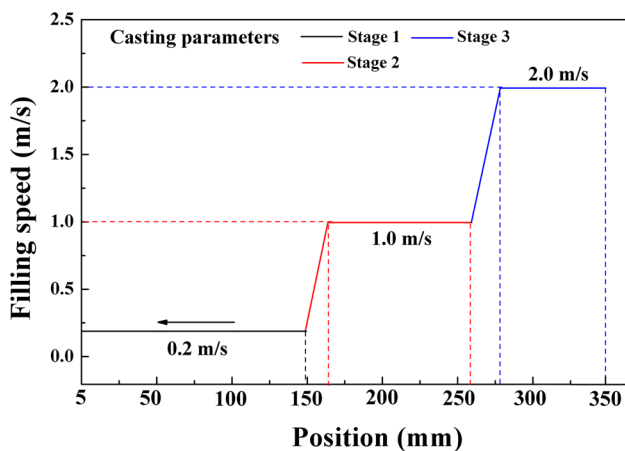
Fig. 4 Casting parameters showing the shot filling speed (mm/s) and filling position (mm) at different stages

extensometer attached to the gauge section of the tensile specimens. For each group of alloys, 5 parallel samples were tested, and then the average YS, UTS, and EL. were calculated.

The specimens for microstructure analysis were cut (from grip areas of tensile specimens), ground, polished, and etched (etchant HF: $H_2O = 0.5$ mL: 100 mL). The etched specimens were observed using a Zeiss optical microscope. Electron backscatter diffraction (EBSD) was applied to

obtain grain size, shape, and orientation. EBSD mapping was performed on a field-emission scanning electron microscope equipped (TESCAN GAIA3) with an EBSD system (Oxford Aztec Nordlys Max3). TSL OIM Analysis 7 software was used to acquire grain orientation maps. The average grain size was measured by linear intercept method according to ASTM E112-12 from at least five independent statistics. A JEOL JSM-6460LA scanning electron microscope equipped with energy-dispersive spectroscopy (EDS) was used to identify the phases and fracture behaviors of the alloys. Transmission electron microscopy (TEM/STEM) analysis was conducted to observe the morphology of Mg_2Si. The thin foil samples for TEM/STEM observations were mechanically grounded to about 160 μm in thickness, and then twin-jet polishing method was applied using a solution of 25% nitric oxide and 75% methanol at temperature of -30 ˚C and voltage of 8 V. Finally, ion beam thinner was applied to expand the thin area of the foil. TEM/STEM observations were performed using a TALOS F200X transmission electron microscope at 200 kV. The area fraction of Mg_2Si phase was calculated using Image-Pro Plus software.

4 Results

## 4.1 Orthogonal Experiments Results

4.1.1 As-Cast Tensile Properties

Fig. 5 shows the tensile properties of the HPDC Al-xMg-ySi-zTi alloys. The YS, UTS, and EL. of the alloys are in the ranges of 197–221 MPa, 354–412 MPa, and 6.2–13.6%, respectively. Figure 5d compares the tensile curves of 4#, 5#, and 6# alloys. It can be observed that different combinations of Mg, Si, and Ti additions lead to significant variations in mechanical properties of the alloys.

4.1.2 ANOVA Results of Orthogonal Experiment

The orthogonal experiment results based on the tensile tests are listed in Table 3, where T_i is the sum of the values of EL., YS, and UTS, respectively, K_i represents the sum of results for the certain factor at level i, S_i is the sum of squares deviations. Table 4 lists the variance analysis of orthogonal test results for the alloys. D is the degree of freedom, and V is mean deviation squares. The significance of the factors is determined by the F-test (at the test level $\alpha = 0.01$, 0.05, 0.1, and 0.25). For EL. of the alloys, the variance analysis results show that $F_{0.1}(2,2) < F_A < F_{0.05}(2,2)$, $F_{0.05}(2,2) < F_B < F_{0.01}(2,2)$, and $F_C < F_{0.25}(2,2)$. Factor B (Si content) has the greatest impact on elongation, followed by factor A. Factor C shows no apparent effect on the elongation since the influence of factor C is within the error range. The

Table 2 Actual chemical compositions of HPDC Al-xMg-ySi-zTi alloys (wt%)

Symbol	Mg	Si	Ti	Mn	Fe	Other	Al
1#	6.41	2.10	0.01	0.68	0.12	<0.3	Bal.
2#	6.43	2.57	0.09	0.67	0.13	<0.3	Bal.
3#	6.46	3.10	0.17	0.65	0.11	<0.3	Bal.
4#	7.02	2.09	0.12	0.71	0.13	<0.3	Bal.
5#	7.10	2.58	0.18	0.66	0.11	<0.3	Bal.
6#	7.06	3.11	0.01	0.71	0.13	<0.3	Bal.
7#	7.54	1.95	0.17	0.69	0.11	<0.3	Bal.
8#	7.51	2.53	0.01	0.68	0.12	<0.3	Bal.
9#	7.49	3.08	0.11	0.72	0.12	<0.3	Bal.
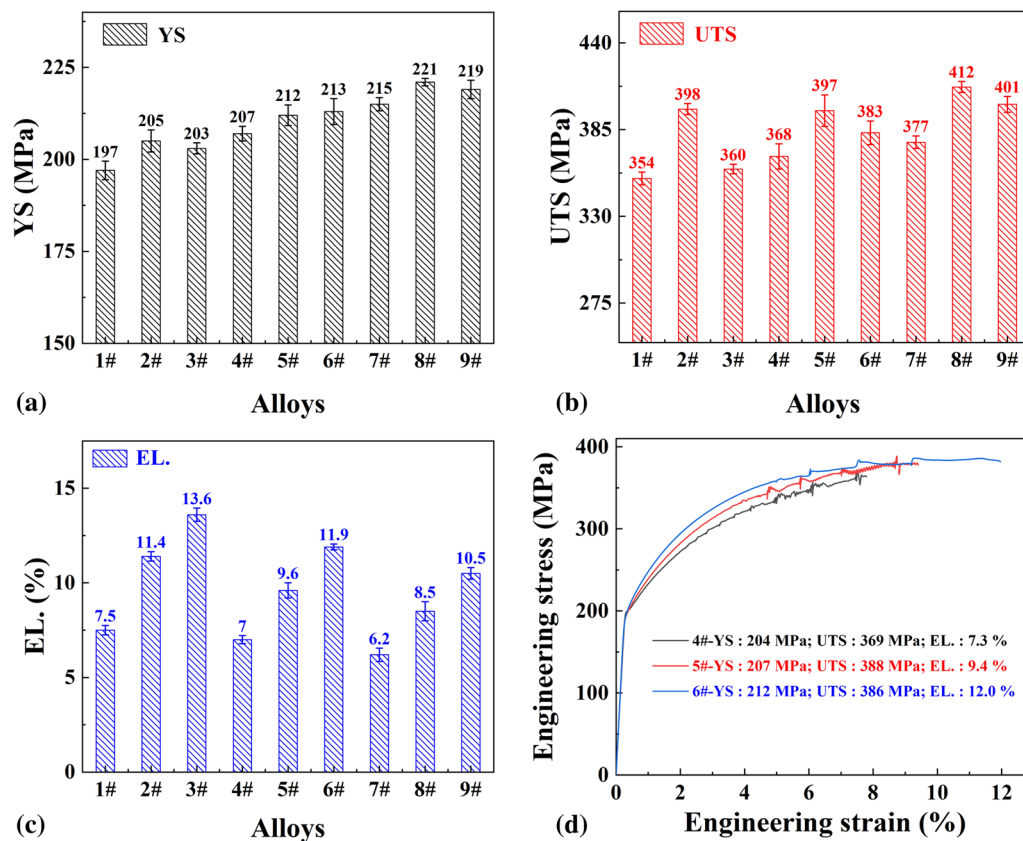
Fig. 5 Tensile properties of HPDC Al-xMg-ySi-zTi alloys **a** YS, **b** UTS, **c** EL and **d** tensile curves of 4#, 5#, and 6# alloys

significance of factors A and B can be signed as "(*)" and "*", respectively.

The variance analysis for YS indicates that factor A (Mg content) has the greatest influence on YS and the significance of factor A can be marked as "**". It is about 99% confidence that Mg content has a significant effect on the YS of the alloys, due to its $F_A > F_{0.01}(2,2)$. Besides, YS is also apparently influenced by factor B, which exhibits 90% confidence. The effects of factors A and B on the UTS exceed the test error. About 95% confidence indicates that Mg and Si content significantly affect UTS. In contrast, the influence of factor C is within the error range. Therefore, no obvious effect on the UTS can be claimed in the present work.

4.1.3 Relationship Between Compositions and Properties

The ANOVA confirms that Mg and Si have an obvious effect on the tensile properties of the alloys. The mathematical relationship between chemical compositions (Mg and Si content) and tensile properties (EL., YS, and UTS) can be simultaneously acquired by multiple regression fitting. The Mg content and Si content are considered as two predictors

Table 3 3 factors and 3 levels orthogonal experiment results

Symbol	A	B	C	D	Results		
	Mg (wt%)	Si (wt%)	Ti (wt%)	e	EL. (%)	YS (MPa)	UTS (MPa)
1#	1 (6.5)	1 (2.0)	1 (0)	1	7.5	197	354
2#	1	2 (2.5)	2 (0.1)	2	11.4	205	398
3#	1	3 (3.0)	3 (0.2)	3	13.6	203	360
4#	2 (7.0)	1	2	3	7.0	207	368
5#	2	2	3	1	9.6	212	398
6#	2	3	1	2	11.9	213	382
7#	3 (7.5)	1	3	2	6.2	215	377
8#	3	2	1	3	8.5	221	412
9#	3	3	2	1	10.5	219	401
K_{1EL}	32.5	20.7	27.9	27.6	$T_{EL.} = 86.2\%$		
K_{2EL}	28.5	29.5	28.9	29.5			
K_{3EL}	25.2	36	29.4	29.1			
S_{EL}	8.9	39.3	0.4	0.7			
K_{1YS}	605	619	631	628	$T_{YS} = 1892$ MPa		
K_{2YS}	632	638	631	633			
K_{3YS}	655	635	630	631			
S_{YS}	417.6	69.6	0.2	4.2			
K_{1UTS}	1112	1099	1148	1153	$T_{UTS} = 3450$ MPa		
K_{2UTS}	1148	1208	1167	1157			
K_{3UTS}	1190	1143	1135	1140			
S_{UTS}	1016	2004.7	172.7	52.7			

Table 4 Variance analysis of orthogonal test results

	Factors	S	D	V (S/D)	F (V_i/V_e)	Significance
EL	A	8.9	2	4.45	12.7	(*)
	B	39.3	2	19.65	56.1	*
	C	0.4	2	0.2	0.57	
	e	0.7	2	0.35		
YS	A	417.6	2	208.8	99.4	**
	B	69.6	2	34.8	16.6	(*)
	C	0.2	2	0.1	0.05	
	e	4.2	2	2.1		
UTS	A	1016	2	508	19.2	*
	B	2004.7	2	1002.5	37.8	*
	C	172.7	2	86.5	3.3	
	e	52.7	2	26.5		

Note: $F_{0.25}(2,2) = 3$, $F_{0.1}(2,2) = 9$, $F_{0.05}(2,2) = 19$, $F_{0.01}(2,2) = 99$

(designated as C_{Mg} and C_{Si}, wt%), and the tensile properties of HPDC Al-xMg-ySi-zTi alloys (EL., YS, and UTS) are defined as the response variable. With the best fitting of test data, the relationship among Mg content, Si content, and tensile properties of the alloys can be expressed as:

$$\text{EL.} = 14.35 - 2.43C_{Mg} + 5.10C_{Si} \quad (R^2 = 0.972) \tag{1}$$

$$\text{YS} = 143.70 + 0.41C_{Mg}^2 - 5.04C_{Si}^2 + 4.32C_{Mg} * C_{Si} \quad (R^2 = 0.992) \tag{2}$$

$$\text{UTS} = 182.52 - 4.77C_{Mg}^2 - 13.55C_{Si}^3 + 37.64C_{Mg} * C_{Si} \quad (R^2 = 0.985) \tag{3}$$

The regression equations can well describe the relationship between predictors and response variables. The results clearly indicate that the appropriate combination of Mg and Si in the alloys can achieve excellent tensile properties. The HPDC Al–Mg–Si–Ti alloys with higher strengths (YS > 200 MPa and UTS > 400 MPa) and better toughness (elongation > 10%) can be developed on the basis of the reasonable combination of the related elements. In this work, the HPDC Al-7.49 Mg-3.08Si-0.01Ti alloy exhibits excellent comprehensive tensile properties (YS of 219 MPa, UTS of 401 MPa, and EL. of 10.5%). The tensile properties, especially UTS of the alloy are higher than the currently reported HPDC Al–Si and Al–Mg alloys [17, 18, 21, 28–30]. The properties of HPDC Al-xMg-ySi-zTi alloys are compared with the typical HPDC Al alloys and displayed in Fig. 6.
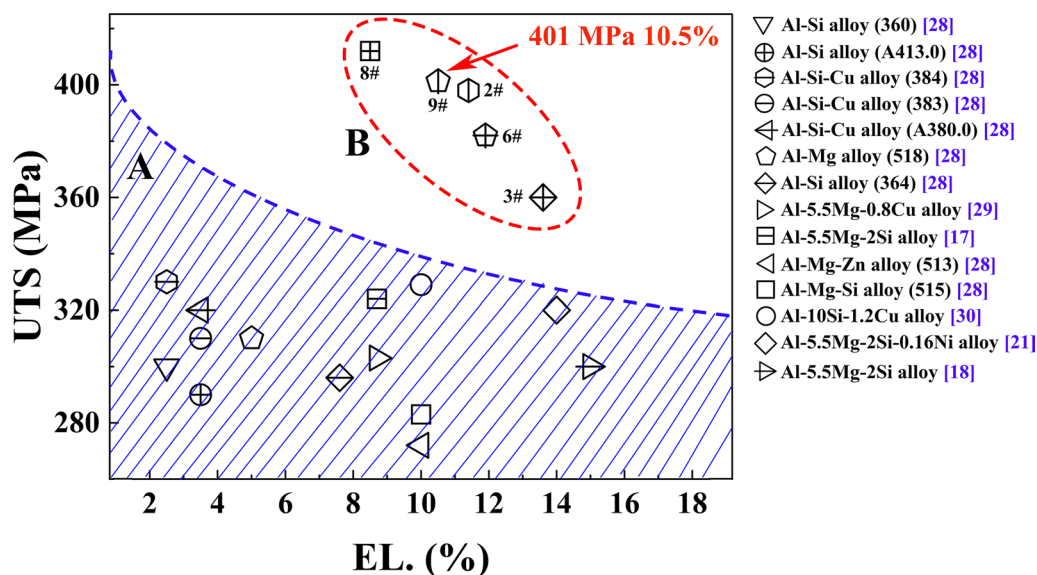
4.2 Microstructures

4.2.1 OM Analysis

The typical optical micrographs (OM) of the HPDC Al-xMg-ySi-zTi alloys (4#: Al-7.0 Mg-2Si-0.15Ti, 5#: Al-7.0 Mg-2.5Si-0.2Ti, 6#: Al-7.0 Mg-3Si-0Ti alloy) are shown in Fig. 7a-c. Referring to the thermal dynamic calculation results, the microstructures mainly consist of α-Al matrix (marked by yellow arrows) and α-Al + Mg$_2$Si eutectic phase (marked by green arrows). The grain size and area fraction of eutectic phase are greatly influenced by the contents of Mg, Si, and Ti. Fig. 7d shows the evolution of area fraction of (α-Al + Mg$_2$Si) eutectic phase with respect to Mg, Si, and Ti content for all 9 alloys. The area fraction of eutectic phase is controlled to be 35.6 to 37.3% when Si addition in the alloys is around 2 wt%, such as 1#, 4#, and 7# alloys. When Si content is increased to 2.5 wt% (2#, 5#, and 8# alloys) and 3 wt% (3#, 6#, and 9# alloys), the area fractions of eutectic phase are reached up to 41.7–45.1% and 50.5–52.3%, respectively.

4.2.2 EBSD and SEM Analysis

Fig. 8 shows EBSD orientation maps and grain size distribution of the HPDC Al-xMg-ySi-zTi alloys (4#, 5#, and 6#). Based on the orientation maps shown in Fig. 8a, c, and e, the grains are randomly oriented. Due to the hybrid nature of the eutectic regions, indexing confidence of these regions is very low. As such, to obtain the grain size of the primary α-Al, the eutectic phase (α-Al + Mg$_2$Si) is marked black in Fig. 8a, c, and e. With the different contents of Si and Ti, the average grain size of 4#, 5#, 6# alloys is in the range of 15.2 μm to 33.5 μm (Fig. 8b, d, and f).

Table 5 summarizes the average grain sizes of the alloys. The average grain sizes of the alloys containing the same Si content but different Ti content are found to be very near. For example, the average grain sizes of the Al-xMg-2.0Si-(0–0.2)Ti alloys are about 32.4 μm (1# alloy), 33.5 μm (4# alloy), and 34.2 μm (7# alloys). Since the eutectic and the matrix content no longer change under a certain addition of Si, it can be speculated that the addition of Ti cannot increase the nucleation density of matrix under the

Fig. 6 Property comparison of HPDC Al-xMg-ySi-zTi alloys with some known non-heat-treated HPDC Al alloys: field A (reported alloys); field B (Al-xMg-ySi-zTi alloys in this work)
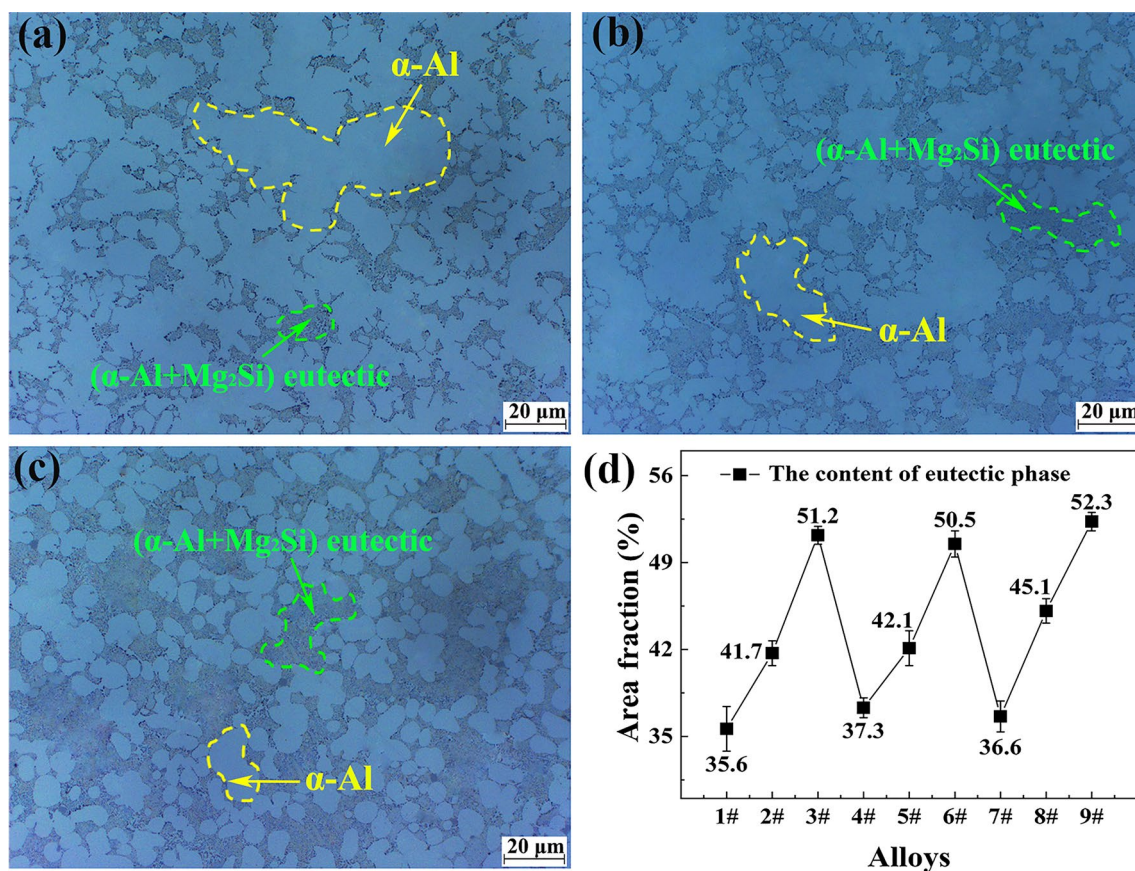
Fig. 7 Optical micrographs of **a** Al-7.0 Mg-2Si-0.15Ti, **b** Al-7.0 Mg-2.5Si-0.2Ti, and **c** Al-7.0 Mg-3Si-0Ti alloys; **d** area fraction of the eutectic phase

fast cooling rate of HPDC. Therefore, the grain refinement potency of Ti is not much effective in this work.

Fig. 9a and b show the typical scanning electron microscopy (SEM) microstructures of the HPDC Al-xMg-ySi-zTi alloys (7#: Al-7.5 Mg-2Si-0.2Ti alloy). Besides the eutectic phase, a few light-white Fe-rich particles distributing along grain boundaries are also observed. In this work, the shape, size (2–3 μm), and area fraction (about 1.31–1.51%) of Fe-containing phase were well controlled by the low Fe content in the alloys and appropriate casting technology. EDS results corresponding to points A (Fig. 9c) and B (Fig. 9d) show that a certain amount of Mg is dissolved in the matrix of the alloy.

Table 6 illustrates Mg concentration in the matrix of the HPDC Al-xMg-ySi-zTi alloys. When Si content in the alloys keeps constant (for example 2 wt% Si), the amount of Mg dissolved in the matrix increases from 3.24 to 4.12 wt% by increasing the total Mg content from 6.5 to 7.5 wt%. Similarly, when the additions of Mg are fixed (such as 6.5 wt% Mg), Mg solid solution in the matrix is decreased from 3.24

to 1.4 wt% with the increase in Si content of the alloys. Therefore, the Mg content dissolved into the matrix mainly determines by the combination of Mg and Si content in the Al-xMg-ySi-zTi alloys.

4.2.3 TEM Analysis

TEM micrographs in Fig. 10(a, b) show the typical morphology of Mg_2Si. Rather than using BF detector for DF imaging, we use an annular detector to obtain the annular dark-field (ADF) image in the STEM mode. The Mg_2Si particles are short rods with elliptical ends. The lengths of the rod-like Mg_2Si particles are in the range of 497.2–1064.7 nm, and the diameters are between 118.1 and 258.8 nm. In this work, the shape and size of Mg_2Si phases are well controlled on the basis of appropriate casting technology. (This part of work will be published in the subsequent papers.) It can be speculated that the fine Mg_2Si particles would guarantee achievement of reasonable mechanical properties of the alloys.
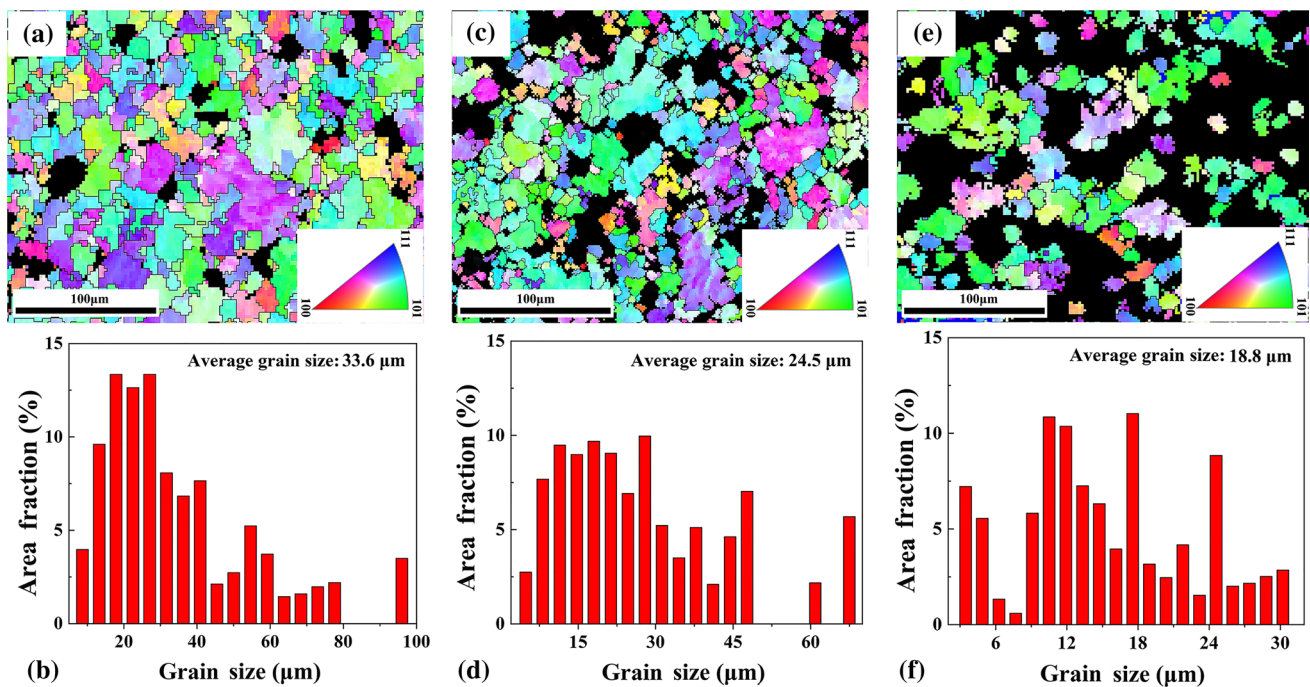
Fig. 8 EBSD orientation map of **a** Al-7.0 Mg-2Si-0.15Ti (4#), **c** Al-7.0 Mg-2.5Si-0.2Ti (5#) and **e** Al-7.0 Mg-3Si-0Ti (6#) alloys; **b, d,** and **f** grain size distributions of 4#, 5#, and 6# alloys, respectively

Table 5 Average grain sizes of HPDC Al-xMg-ySi-zTi alloys

Alloys	Size (μm)	Alloys	Size (μm)	Alloys	Size (μm)
1#	32.4 ± 5.4	4#	33.6 ± 4.2	7#	32.2 ± 3.0
2#	23.5 ± 3.2	5#	24.5 ± 2.1	8#	25.2 ± 3.5
3#	16.1 ± 1.5	6#	18.8 ± 2.3	9#	17.3 ± 1.8

$$S\text{m} = 56.88 + 0.90C_{\text{Mg}} - 15.33C_{\text{Si}} \quad \left(R^2 = 0.983\right) \tag{4}$$

$$E = -7.42 + 2.00C_{\text{Mg}} + 14.77C_{\text{Si}} \quad \left(R^2 = 0.987\right) \tag{5}$$

$$M = 0.21 + 0.96C_{\text{Mg}} - 1.71C_{\text{Si}} \quad \left(R^2 = 0.993\right) \tag{6}$$

4.2.4 Relationship of Compositions and Microstructures

Based on the OM and SEM observations, it can be inferred that Mg and Si additions in the alloys induce variations in the eutectic phase, average grain size, and degree of Mg solid solution. The microstructural characteristics of the alloys depend obviously on the contents of Mg and Si. Besides, the contents of eutectic phase and matrix are closely related to each other. Therefore, the area ratio of eutectic to matrix is used to represent the relative content of eutectic phase in this paper. To calculate the average grain size, area fraction of eutectic phase, and content of Mg dissolved into matrix, multiple regression analyses are used to obtain the mathematical relationship among grain size (designated as Sm, μm), Mg content in the matrix (designated as M, wt%), relative fraction of eutectic (designated as E, %), and chemical compositions (C_{Mg}, C_{Si}, wt%) of the HPDC Al-xMg-ySi-zTi alloys. The mathematical relationship can be expressed as:

The results indicate that the formula can effectively describe the relationship between chemical compositions and microstructures characteristics. The area fraction of eutectic phase and the average grain sizes are mainly decided by the content of Si. The solid solubility of the matrix in the alloys is determined by both Mg and Si content. Besides, the microstructures predicted by Pandat software are similar to the experimental results. The thermal dynamic calculation is also able to gain the solidification range of different alloys. Therefore, it provides important guidelines for the development of HPDC Al–Mg–Si–Ti alloys.

4.2.5 Relationship between Microstructures and Properties

The average grain size, area fraction of eutectic phase, and the content of Mg dissolved into the matrix result in the diversities in the mechanical properties of the alloys. Thus, the relationship between microstructures and properties needs to be further explored. Table 7 shows the variations of
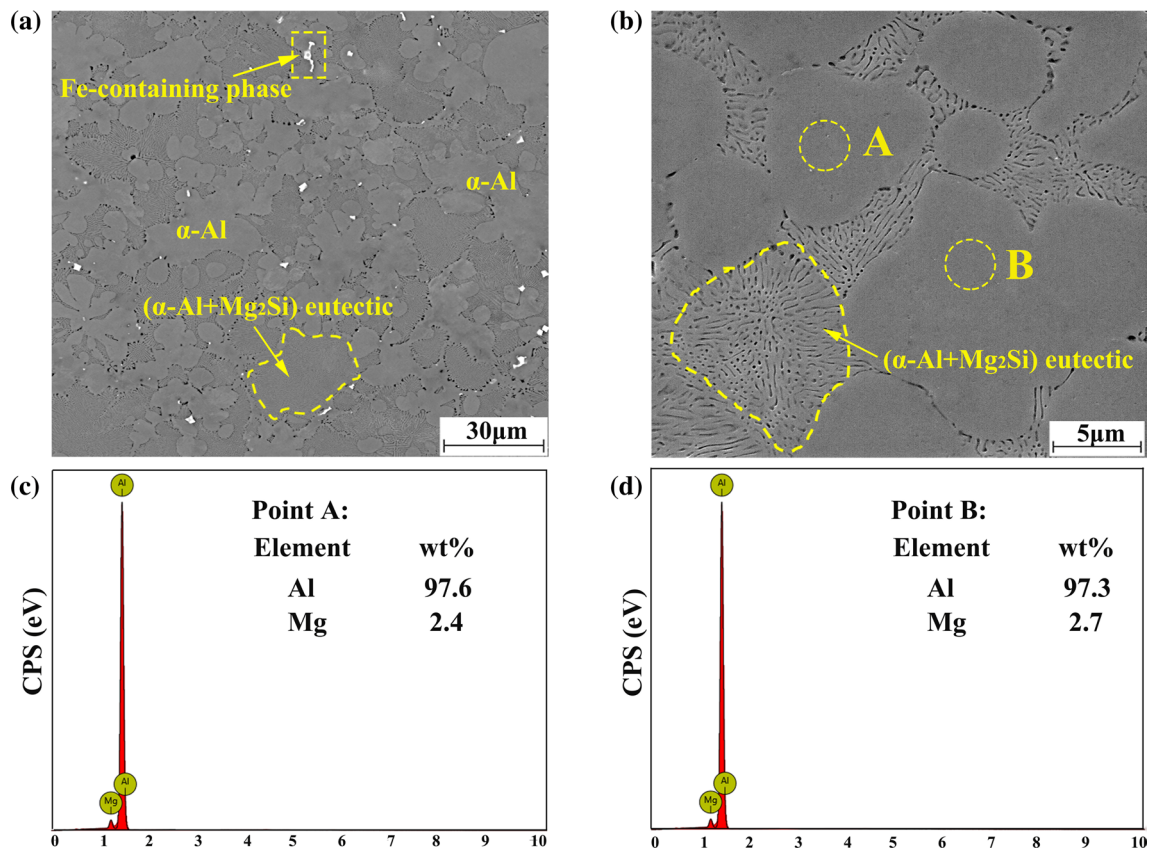
Fig. 9 **a** and **b** SEM images showing microstructures of HPDC Al-xMg-ySi-zTi alloys; **c** and **d** EDS results corresponding to points A and B in **b**

the microstructures and tensile properties of HPDC Al-xMg-ySi-zTi alloys in comparison with 1# alloy (as a baseline).

The multiple regression analysis was conducted between predictors (ΔM, ΔSm, and ΔE) and response variables (ΔEL., ΔYS, and ΔUTS). The relationship between the increment of microstructures and variation of tensile properties of the alloys can be expressed as follows:

$$\Delta EL. = 0.59 - 0.25\Delta Sm - 2.04\Delta M - 4.55\Delta E \quad \left(R^2 = 0.930\right) \tag{7}$$

$$\Delta YS = 1.45 - 2.13\Delta Sm + 18.98\Delta M + 10.91\Delta E \quad \left(R^2 = 0.918\right) \tag{8}$$

F-test is used to check the significance of each regression coefficient in Eqs. (7–9). It confirms the influence degree of the predictors (ΔE, ΔSm, and ΔM) on the response variable (ΔEL., ΔYS, and ΔUTS), and thus the primary and secondary predictors influencing the change of response variables are identified. F values for ΔE, ΔSm, and ΔM on Eqs. (7–9) are listed in Table 8. The influence degree is determined at a defined significant level of $\alpha = 0.05$ and 0.1.

The order of F value for ΔEL. is confirmed as $F_{\Delta M} > F_{0.05} > F_{\Delta Sm} > F_{0.1} > F_{\Delta E}$. Hence, it is believed that ΔEL. value is mainly determined by ΔM and ΔSm ($\Delta M > \Delta Sm$). The change of Mg content in the matrix has the most sig-

$$\Delta UTS = 1.74 - 1.87\Delta Sm + 124.3\Delta E + 23.03\Delta M^2 - 10.95\Delta Sm * \Delta M * \Delta E \quad \left(R^2 = 0.951\right) \tag{9}$$

Table 6 Average concentration of Mg in the matrix of HPDC Al-xMg-ySi-zTi alloys measured by SEM–EDS

Alloys	Mg (wt%)	Alloys	Mg (wt%)	Alloys	Mg (wt%)
1#	3.24 ± 0.14	4#	3.74 ± 0.29	7#	4.12 ± 0.26
2#	2.44 ± 0.20	5#	2.91 ± 0.17	8#	3.31 ± 0.16
3#	1.40 ± 0.13	6#	2.11 ± 0.32	9#	2.47 ± 0.30

nificant effect on the elongation of the alloys. In addition, average grain size also influences the ductility of the alloys. F value for ΔYS indicates that the yield strength of the alloys is determined mainly by the content of Mg in the matrix and the average grain size. The content of Mg in the matrix has a greater influence on the YS in comparison with average grain size of the alloys. For ΔUTS of the alloys, F value is confirmed as $F_{\Delta E * \Delta Sm * \Delta M} > F_{\Delta M}^2 > F_{\Delta E} > F_{0.05} > F_{\Delta Sm} > F_{0.1}$.
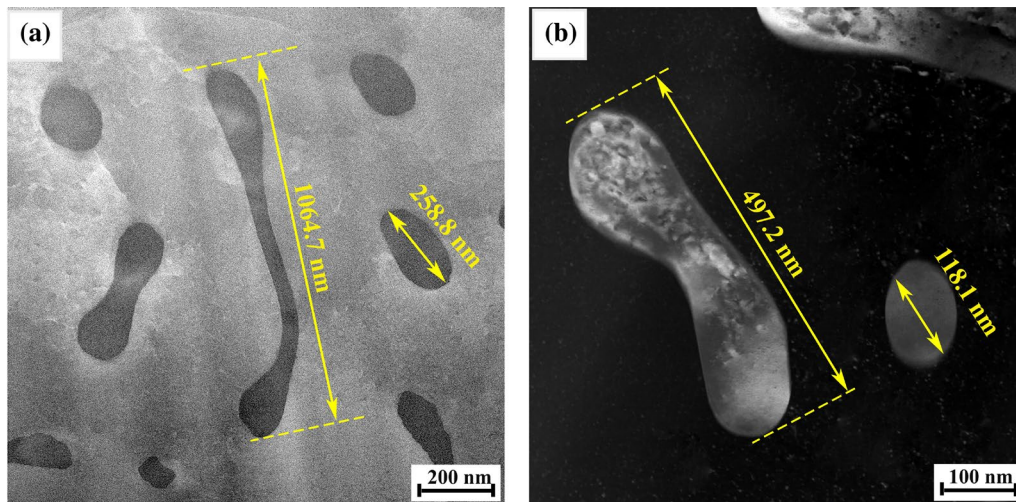
Fig. 10 TEM micrographs of Mg_2Si phase: **a** bright-field and **b** annular dark-field image

Table 7 Variations of the microstructures and properties of HPDC Al-xMg-ySi-zTi alloys in comparison with 1# alloy

Alloys	ΔE	ΔSm (µm)	ΔM (wt%)	$\Delta EL.$ (%)	ΔYS (MPa)	ΔUTS (MPa)
1#	0	0	0	0	0	0
2#	0.18	−8.9	−0.80	3.9	8	42
3#	0.52	−16.3	−1.84	6.1	6	6
4#	0.04	1.2	0.50	−0.5	10	12
5#	0.23	−7.9	−0.33	2.1	15	42
6#	0.49	−13.6	−1.13	4.4	16	28
7#	0.03	−0.2	0.88	−1.3	18	23
8#	0.30	−7.2	0.07	1	22	55
9#	0.57	−15.1	−0.77	3	24	45

Table 8 F values for ΔE, ΔSm, and ΔM on the Eqs. (7–9)

Properties/F	ΔE	ΔSm	ΔM	ΔM^2	$\Delta E*\Delta Sm*\Delta M$
ΔEL	2.71	4.12	20.32	–	–
ΔYS	1.22	23.00	137.23	–	–
ΔUTS	15.20	4.49	–	15.84	52.98

Note: $F_{0.05}(1,5) = 6.61$, $F_{0.1}(1,5) = 4.06$

Solid solution atom in the matrix, eutectic phase content, and average grain size influence obviously the ultimate tensile strength of the alloys, especially the interaction effect of $\Delta E*\Delta Sm*\Delta M$.

4.3 Fracture Behavior

To explore the fracture behavior of the alloys, microstructures near the fracture surface of the specimens are observed through SEM. The typical microstructures of the as-cast alloys are shown in Fig. 11, where three types of cracks can be identified, *i.e.,* cracks originating at the Fe-containing phase (Fe-cracks), eutectic phase (E-cracks), or matrix–eutectic interface (E-M-cracks).

Fig. 12 further shows the area fraction of the cracked phases near the fracture of the alloys. When Mg content is constant (for example, 1–3# alloys, 6.5 wt% Mg), the ratio of the M-E cracks decreases (from 31 to 8%), and the contents of the Fe-cracks increase (from 61 to 88%) with the addition of Si in the alloys from 2 to 3 wt%. Conversely, when Si content is kept constant (for example, 1#, 4#, 7# alloys, 2 wt% Si), the ratio of the M-E cracks increases (from 31 to 47%), and the contents of the Fe-cracks decrease (from 61 to 45%) with the addition of Mg in the alloys from 6.5 to 7.5 wt%.

In the present work, 1# (31%), 4# (39%), 5# (25%), 7# (47%), and 8# (28%) alloys include more E-M-cracks and 2# (72%), 3# (88%), 6# (82%), and 9# (73%) alloys contain more Fe-cracks. Moreover, the results also show that the ratio of the E-cracks in the alloys is maintained at a low level. It is believed that the content and type of cracks are closely related to microstructure characteristics of HPDC Al-xMg-ySi-zTi alloys.
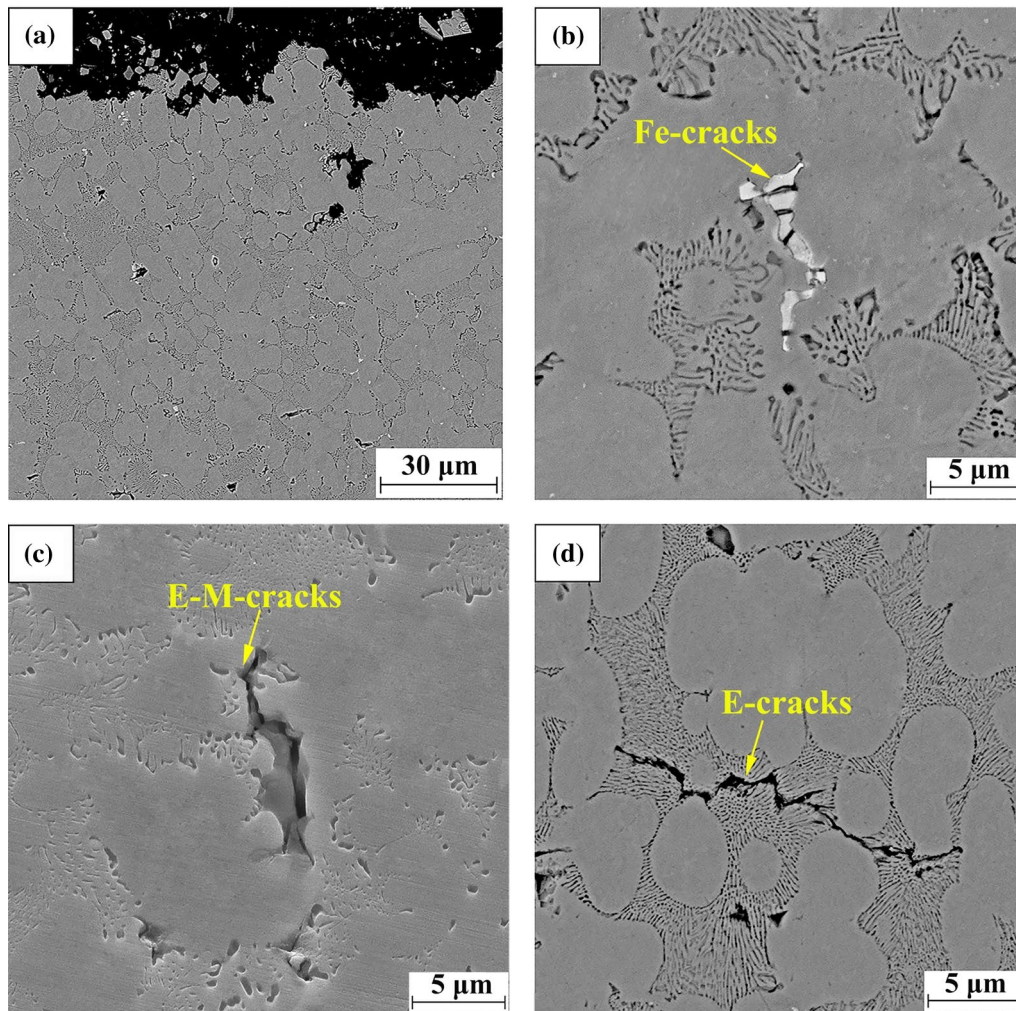
Fig. 11 SEM images showing microstructures near the fracture surface of the HPDC Al-*x*Mg-*y*Si-*z*Ti alloys specimens: **a** near the fracture surface; **b** Fe-cracks; **c** E-M-cracks; **d** E-cracks
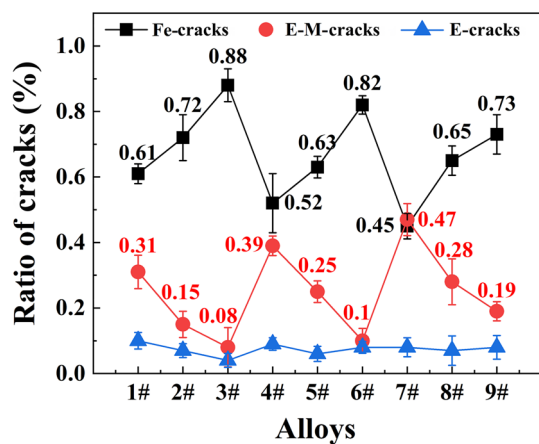
Fig. 12 Ratio of cracks (including Fe-cracks, E-M-cracks, and E-cracks) near the fracture of the HPDC Al-*x*Mg-*y*Si-*z*Ti alloys

In addition, Fig. 12 also shows that the Fe-cracks is the most influencing factor in the fracture behavior and mechanical properties. In this paper, the content of Fe is controlled below 0.15 wt%. The Fe content is treated as an invariant, and the content of Fe in the nine alloys is quite near. In addition, the shape, size, and area fraction of Fe-containing phases maintained similar in all alloys. Therefore, it can be concluded that the effect of Fe on fracture behavior among the nine alloys is similar. Because of the design of the alloys, the ratio of the Fe-cracks and E-M-cracks changes during deformation. For the alloys with elongation > 10%, the proportion of Fe-cracks is high. In addition to Fe-cracks, E-M-cracks also become the main cracking sources for the alloys with relatively low elongation (< 10%).
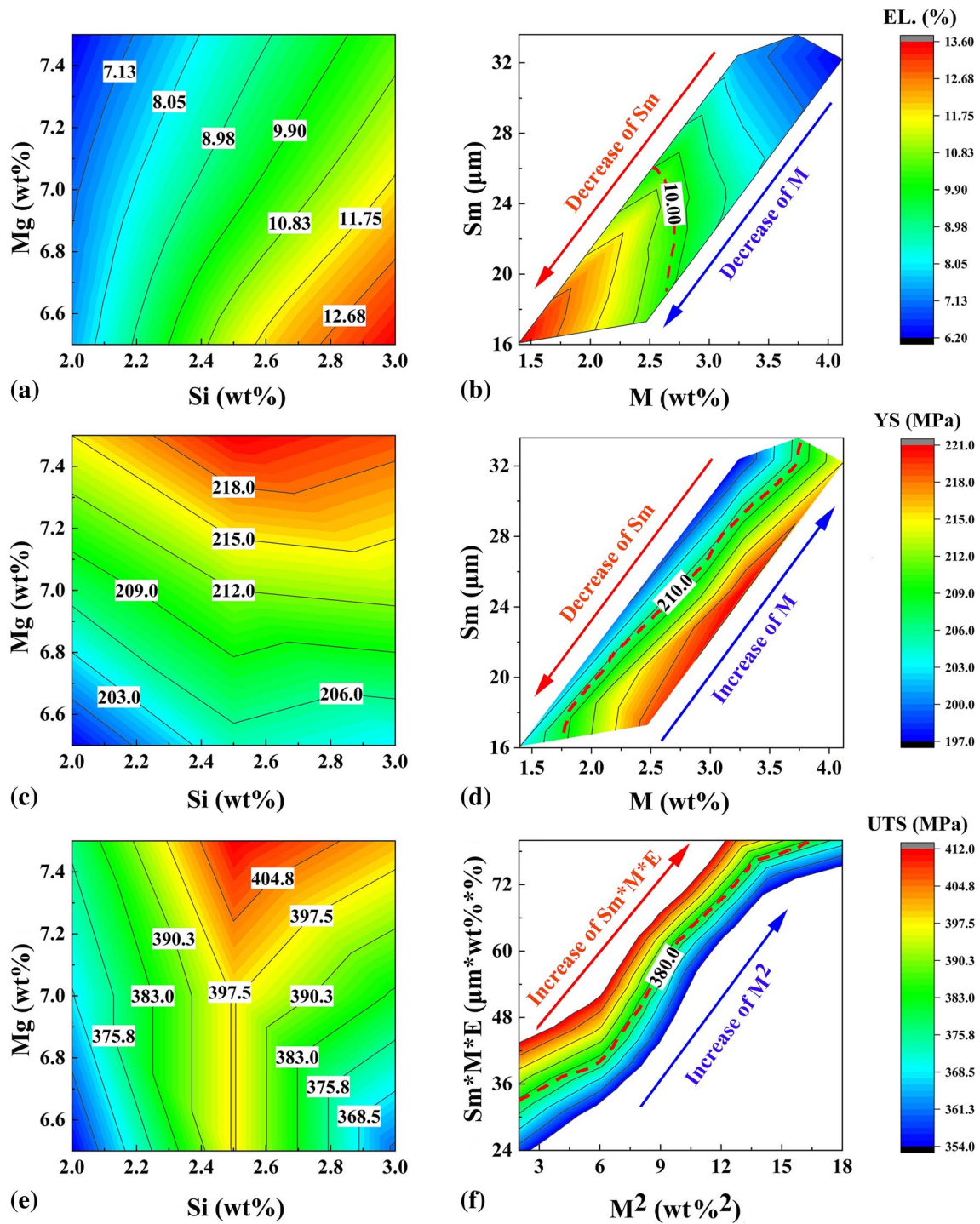
Fig. 13 Contour maps of EL., YS, UTS versus the contents of Mg, Si, and the microstructure: **a** Mg and Si-EL.; **b** average grain size (*S*m) and Mg content in the matrix (*M*)-EL.; **c** Mg and Si-YS; **d** average grain size (*S*m) and Mg content in the matrix (*M*)-YS; **e** Mg and Si-UTS; **f** average grain size (*S*m), Mg content in the matrix (*M*) and eutectic phase content (*E*)-UTS

5 Discussion

5.1 Key Affecting Factors for HPDC Al–Mg–Si Alloy

In the present study, nine alloys with different chemical compositions were designed, and their microstructures were characterized. Based on these microstructural characterizations, the variations in the tensile properties were investigated through orthogonal test method. The tensile properties processed by HPDC can be predicted by Eqs. (1–3). The relationship between microstructures (solubility, grain size, and eutectic phase) and chemical compositions can be expressed by using Eqs. (4–6). Furthermore, the quantitative relationship between microstructures and tensile properties is illustrated by Eqs. (7–9). Therefore, it can be inferred that Eqs. (1–9) provide effective guidelines for developing high-strength and high-ductility HPDC Al–Mg–Si–Ti alloys.

By utilizing Eqs. (1–9), contour maps of EL., YS, UTS versus contents of Mg and Si, and the microstructural characterizations are shown in Fig. 13. The combination of Mg and Si effectively determines the tensile properties of the alloys (Fig. 13a, c, and e). For example, to gain higher elongation, simultaneous alteration of Mg and Si content are more effective than changing a single element (Fig. 13a). When the Mg content is selected between 6.5–7.5 wt%, it is necessary to regulate the contents of Si in the range of 2.4–3.0 wt% to obtain higher elongation (> 10%). Fig. 13a provides out the ranges of element content to obtain ductile Al–Mg–Si–Ti alloys. For YS and UTS, Fig. 13c and e give corresponding guidance. However, it should be noted that the effects of Mg and Si on EL. and YS possess monotonicity among the nine alloys experiment (as shown in Fig. 13a and c). The EL. and YS of the alloys at different levels of one factor are not affected by the levels of another factor. Therefore, there is no interaction between factor *A* and factor *B* for EL. and YS in this work. The results in Fig. 13e indicate that the UTS of the alloys is strongly affected by the interaction of Mg and Si. Furthermore, the influence of one factor or level on the UTS of the alloys is restricted by another. In addition, it is noted that the YS, EL., and strain hardening of alloys have a significant effect on the UTS of the alloys. On the other hand, the YS of an alloy represents weight loss, and the EL. indicates the ambient connection for Al car body structural components. Thus, it is not appropriate to consider the UTS of the alloy separately in this work. A more rigorous treatment needs to be completed for 27 alloy compositions ($L_{27}(3^{13})$) to obtain the interaction between Mg and Si on the UTS of the alloys. Considering the results obtained by $L_9(3^3)$ orthogonal experiment, as well as the time and alloy development cost, authors believe that the current results are sufficient to achieve the aim of this research work.

Mechanical properties of the alloys are closely related to the difference of microstructures, as shown in Fig. 13b, d, and f, which are associated with the chemical compositions. The content of Mg in the matrix (determined by Mg and Si content) and average grain size (depend on the Si content) have the most significant effect on EL. and YS. Fig. 13b and d reveal the quantitative relationship of Mg content in the matrix (*M*), average grain size (*Sm*), EL., and YS of the alloys. According to the results, it can be inferred that the alloy with 2.0 wt% Mg content in the matrix and average grain size of 20 μm would gain an elongation value of higher than 10% and yield strength of ~ 210 MPa. For the UTS of the alloys, both *M*, *Sm*, and eutectic phase content E (depend on the Si content) influence the UTS, especially the interaction effect of *E*, *Sm*, and *M*. Fig. 13f shows the relationship between the two most obvious factors and UTS. The increase in M^2 and Sm*M*E can improve the UTS to 380 MPa. It is clear that the contour maps established by the relationship among chemical composition, microstructures, and tensile properties offer a novel strategy to guide the development of high-strength and high-ductility HPDC Al–Mg–Si alloys for the application of car body structural components and uncover a broader field to be explored.

5.2 Strengthening and Toughening Mechanism of the Alloys

The results mentioned above have shown the different combinations of the alloying elements, and contents lead to variation in the average grain size, the contents of eutectic phase, and Mg dissolved into the Al matrix, which are considered as the most important microstructural parameters for HPDC Al-*x*Mg-*y*Si-*z*Ti alloys. The interaction of solubility, grain size, and second phase determines the mechanical properties.

According to Eq. 7, the content of Mg in the matrix and average grain size influence the ductility of the Al-*x*Mg-*y*Si-*z*Ti alloys. The alloys (2#, 3#, 6#, and 9#) with Mg content in the matrix (1.4–2.4 wt%) and average grain size (16.1–23.5 μm) trend to gain better elongation (> 10%). Combined with the fracture features shown in Fig. 11, it can be speculated that the finer α-Al with lower Mg solid solution in these alloys can reduce stress concentration and homogenize the stress distribution along the grain boundary. The cracks mainly originate from the hard-brittle Fe-containing phase distributed along the grain boundary even with the higher content of eutectic phase. In this work, the content of Fe is controlled to be 0.1–0.15 wt%, and Mn is added to change the morphology and size of Fe-containing phase to minimize the harmful effect of the Fe-rich phase on elongation. Therefore, the alloys (2#, 3#, 6#, and 9#) with lower Mg content in the matrix and finer grain size have the higher ductility. In contrast, the alloys (1#, 4#, 5#, 7# and

8#) containing higher Mg content (2.92–4.12 wt%) in the matrix and larger average grain size (24.5–33.6 μm) exhibit more E-M-cracks during fracture. It is believed that the larger grain size and the strong solid solution strengthening result in the stress concentration around the grain boundary. In addition to the Fe-cracks, matrix–eutectic interface also becomes the main crack source of crack propagation during tensile tests. Once E-M cracks occur, the matrix–eutectic interfaces around them provide favored routes for crack growth, leading to significant decrease in elongation, as revealed by the length of E-M cracks and Fe-cracks shown in Fig. 11b and c.

For the YS of the alloys, the Mg content dissolved into the matrix and average grain size has the most significant effect. The finer α-Al along with higher Mg solid solution leads to superior YS due to stronger solid solution strengthening and grain boundary strengthening. In this work, 5–9# alloys obtain higher YS (> 210 MPa) with the Mg content dissolved into the matrix being 2.11–4.12 wt% and average grain size of 17.3–32.2 μm. The 8# alloy with higher solid solution atoms in the matrix (2.9 wt%) and finer average grain size (25.2 μm) achieves the highest YS (221 MPa) among all the alloys. The results indicate that the coordination of solid solution strengthening and grain boundary strengthening largely determines the YS of HPDC Al-xMg-ySi-zTi alloys. Similarly, the mutual coordination of Mg dissolved into the matrix (solid solution strengthening), eutectic phase (dispersion strengthening), and grain size (grain boundary strengthening) determines the UTS of the alloys. The 2#, 5#, 8#, and 9# alloys with 2.44–3.31 wt% Mg content in the matrix, average grain size of 17.3–25.2 μm, and eutectic phase in a range of 41.7–52.3% exhibit UTS of 400 MPa. Besides, it is interesting that the content of the E-cracks is maintained at a low level, indicating that the eutectic phase, especially fine Mg_2Si particles (shown in Fig. 10), can strengthen the alloys with limited damage to elongation.

6 Conclusions

In this work, the effects of Mg (6.5–7.5 wt%), Si (2.0–3.0 wt%), and Ti (0–0.2 wt%) on the microstructure and tensile properties of HPDC Al-xMg-ySi-zTi alloys were investigated. The multiple regression analysis toward the experimental data was further conducted to reveal the relationship between compositions, microstructure, and tensile properties. The following conclusions can be drawn:

1. According to the variance analysis of the orthogonal experimental design, both Mg and Si content apparently influence the mechanical properties of HPDC Al-xMg-ySi-zTi alloys. Among these alloys, the Al-7.49 Mg-

3.08Si-0.01Ti alloy exhibits an optimum combination of strength and ductility, with YS of 219 MPa, UTS of 401 MPa, and EL. of 10.5%.

2. The additions of Mg, Si, and Ti elements in the alloys result in the variation of eutectic phase from 35.6 to 52.3%, average grain size from 16.1 to 33.6 μm, and Mg solid solution in the matrix from 1.4 to 4.12 wt%, respectively. In contrast, Ti content does not show any considerable effects on the average grain size of the HPDC alloys.

3. When the Mg solid solution content is < 2.47 wt% and the average grain size is < 23.5 μm, plasticity of the HPDC alloys increases to be > 10%, which is mainly attributed to less E-M cracks during tensile tests. The coordination of Mg solid solution content (2.11–4.12 wt%) and the average grain size (17.3–32.2 μm) obtains YS > 210 MPa. The combination of the 2.44–3.3 wt% Mg solid solution content, the average grain size 17.3–25.2 μm, and the 41.7–52.3% eutectic phase gains high UTS ~ 400 MPa.

4. The contour maps established by the relationship among chemical compositions, fraction of eutectic phase, average grain size, Mg solid solution, and tensile properties (YS of 197–221 MPa, UTS of 354–412 MPa, EL. of 6.2–13.6%) can be used as guidelines for the development of high strength and toughness HPDC Al–Mg–Si alloys.

References

[1] A.I. Taub, A.A. Luo, Advanced lightweight materials and manufacturing processes for automotive applications. MRS Bull. **40**, 1045 (2015)

[2] G.S. Cole, A.M. Sherman, Light weight materials for automotive applications. Mater. Charact. **35**, 3 (1995)

[3] A. Morita, Aluminum alloys for automobile applications, Proceedings of the 6th International Conference on Aluminum Alloys (Proc. 6th ICAA) **1**, 25 (1998)

[4] W.S. Miller, L. Zhuang, J. Bottema, A.J. Wittebrood, P.D. Smet, A. Haszler, A. Vieregge, Recent development in aluminium alloys for the automotive industry. Mater. Sci. Eng. A **280**, 37 (2000)

[5] J.T. Staley, D.J. Lege, Advances in aluminium alloy products for structural applications in transportation. Le J. de Phys. IV. **3**, 179 (1993)

[6] S. Ji, Light-Weighted Materials for Automotive Industry. BCAST Internal Report (Brunel University, UK, 2011).

[7] G. Davies, Materials for Automobile Bodies, 2nd edn. (Butterworth-Heinemann, Oxford, 2012).

[8] J.G. Kaufman, E. Rooy, Aluminum Alloy Castings: Properties, Processes, and Applications, 1st edn. (ASM International, US, 2004).

[9] X. Dong, H. Yang, X. Zhu, S. Ji, High strength and ductility aluminium alloy processed by high pressure die casting. J. Alloy Compd. **773**, 86 (2019)

[10] S. Ji, F. Yan, Z. Fan, Development of a high strength Al–Mg2Si–Mg–Zn based alloy for high pressure die casting. Mater. Sci. Eng. A **626**, 165 (2015)

[11] F. Yan, W. Yang, S. Ji, Z. Fan, Effect of solutionising and ageing on the microstructure and mechanical properties of a high strength die-cast Al–Mg–Zn–Si alloy. Mater. Chem. Phys. **167**, 88 (2015)

[12] V.S. Zolotorevsky, N.A. Belov, M.V. Glazoff, Casting Aluminum Alloys, 1st edn. (Elsevier, Oxford, 2007).

[13] F. Bonollo, N. Gramegna, G. Timelli, High-pressure die-casting: Contradictions and challenges. JOM **67**, 901 (2015)

[14] F. Casarotto, A.J. Franke, R. Franke, Advanced Materials in Automotive Engineering, 1st edn. (Woodhead, Cambridge, 2012).

[15] S. Ji, H. Yang, X. Cui, Z. Fan, Macro-heterogeneities in microstructures, concentrations, defects and tensile properties of die cast Al–Mg–Si alloys. Mater. Sci. Technol. **33**, 2223 (2017)

[16] P. Zhang, Z. Li, B. Liu, W. Ding, L. Peng, Improved tensile properties of a new aluminum alloy for high pressure die casting. Mater. Sci. Eng. A **651**, 376 (2016)

[17] Z. Hu, L. Wan, S. Wu, H. Wu, X. Liu, Microstructure and mechanical properties of high strength die-casting Al–Mg–Si–Mn alloy. Mater. Des. **46**, 451 (2013)

[18] S. Ji, D. Watson, Z. Fan, M. White, Development of a super ductile diecast Al–Mg–Si alloy. Mater. Sci. Eng. A **556**, 824 (2012)

[19] H. Koch, B. Lenczowski, Al/Mg/Si Cast Aluminium Containing Scandium. E. U. Patent 2005/047554, 26 May 2005

[20] G. Trenda, A. Kraly, Aluminum alloy. US Patent 8,337,644, 25 Dec 2012

[21] H. Yang, D. Watson, Y. Wang, S. Ji, Effect of nickel on the microstructure and mechanical property of die-cast Al–Mg–Si–Mn alloy. J. Mater. Sci. **49**, 8412 (2014)

[22] S. Ji, W. Yang, F. Gao, D. Watson, Z. Fan, Effect of iron on the microstructure and mechanical property of Al–Mg–Si–Mn and Al–Mg–Si diecast alloys. Mater. Sci. Eng. A **564**, 130 (2013)

[23] U. Hielscher, H. Sternau, H. Koch, R. Klos, New developed pressure die casting alloy with excellent mechanical properties in the as-cast condition. Giesserei **85**, 62 (1998)

[24] U. Hielscher, H. Sternau, H. Koch, A. Franke, Magsimal-59, an AlMgMnSi-type squeeze-casting alloy designed for temper F. Paper presented at the 125th annual meeting and exhibition of the Minerals, Metals and Materials Society, California, US, 4-8th February 1996

[25] S. Otarawanna, C.M. Gourlay, H.I. Laukli, A.K. Dahle, Microstructure formation in AlSi4MgMn and AlMg5Si2Mn high-pressure die castings. Metall. Mater. Trans. A **40**, 1645 (2009)

[26] S. Ji, Y. Wang, D. Watson, Z. Fan, Microstructural evolution and solidification behavior of Al-Mg-Si alloy in high-pressure die casting. Metall. Mater. Trans. A **44**, 3185 (2013)

[27] N.A. Belov, D.G. Eskin, A.A. Aksenov, Multicomponent Phase Diagrams: Applications for Commercial Aluminum Alloys. (Elsevier, Oxford, 2005)

[28] D.M. Stefanscu, J.R. Davis, J.D. Destefani (Eds.), ASM Metals Handbook, Casting. Vol. 15, 9th edn. (ASM International, US, 1998)

[29] L. Yuan, L. Peng, J. Han, B. Liu, Y. Wu, J. Chen, Effect of Cu addition on microstructures and tensile properties of high-pressure die-casting Al-5.5 Mg-0.7 Mn alloy. J. Mater. Sci. Technol. **35**, 1017 (2019)

[30] P. Zhang, Z. Li, B. Liu, W. Ding, Tensile properties and deformation behaviors of a new aluminum alloy for high pressure die casting. J. Mater. Sci. Technol. **33**, 367 (2017)